PERGAMON

International Journal of Heat and Mass Transfer 42 (1999) 685–695

International Journal of HEAT and MASS TRANSFER

Analysis of laminar mixed-convection condensation on isothermal plates using the full boundary-layer equations: mixtures of a vapor and a lighter gas

V. Srzic, H. M. Soliman*, S. J. Ormiston

Department of Mechanical and Industrial Engineering, University of Manitoba, Winnipeg, Manitoba, Canada R3T 5V6

Received 4 December 1997; in final form 10 June 1998

Abstract

Laminar film condensation from mixtures of a vapor and a lighter noncondensable gas flowing downward along inclined isothermal plates is investigated numerically using the full boundary-layer equations for the liquid film and the mixture. The adverse net body force due to high concentration of the lighter gas near the liquid–mixture interface gives rise to the possibility of boundary-layer separation. A numerical solution was developed based on a finite-control-volume method and it was marched along the plate up to the separation location. Results were obtained for three vapor–gas mixtures covering a wide range of liquid Prandtl numbers, high gas concentration and high liquid subcooling. Comparisons with previous models (which included various simplifying assumptions) showed that agreement is possible only for conditions of low gas concentration and liquid subcooling. Results of the separation distance exhibited interesting trends, which are discussed and explained. It is also demonstrated that lighter gases can have a more inhibiting effect on heat transfer than heavier gases.

Nomenclature

C_P specific heat [$J \cdot kg^{-1} \cdot K^{-1}$]
D diffusion coefficient [$m^2 \cdot s^{-1}$]
e_1, e_2 relative errors, equation (22)
g gravitational acceleration [$m \cdot s^{-2}$]
h_{fg} latent heat of vaporization [$J \cdot kg^{-1}$]
Ja Jakob number ($=C_p \Delta T/h_{fg}$)
k thermal conductivity [$W \cdot m^{-1} \cdot K^{-1}$]
$\dot{m}$ mass flow rate per unit depth [$kg \cdot m^{-1} \cdot s^{-1}$]
$\dot{m}''$ mass flux [$kg \cdot m^{-2} \cdot s^{-1}$]
Nu_x local Nusselt number, equation (24b)
P pressure [$N \cdot m^{-2}$]
Pr Prandtl number ($=\mu C_p/k$)
q local wall heat flux [$W \cdot m^{-2}$]
R gas constant [$J \cdot kg^{-1} \cdot K^{-1}$]
Re_x local Reynolds number, equation (24c)
Re_δ film Reynolds number, equation (18)
T temperature [K]
ΔT overall temperature difference ($=T_\infty - T_{wall}$) [K]
u velocity in the x direction [$m \cdot s^{-1}$]
v velocity in the y direction [$m \cdot s^{-1}$]
W gas mass fraction
x coordinate along the plate [m]
x^* dimensionless coordinate along the plate, equation (23)
y coordinate normal to the plate [m].

Greek symbols

Γ film flow rate per unit depth [$kg \cdot m^{-1} \cdot s^{-1}$]
δ film thickness [m]
δ_T, δ_u, δ_W thermal, hydrodynamic, and concentration boundary layer thicknesses [m]
η transformed coordinate normal to the plate, equation (21)
θ angle of plate inclination [radians]
μ viscosity [$N \cdot s \cdot m^{-2}$]
ν kinematic viscosity [$m^2 \cdot s^{-1}$]
ρ density [$kg \cdot m^{-3}$]
σ condensation coefficient, equation (15)
τ shear stress [$N \cdot m^{-2}$]
ϕ general variable, equation (22)
χ transformed coordinate along the plate, equation (21).

* Corresponding author

0017–9310/98 $19.00
PII: S0017–9310(98)00198–7

Subscripts
g gas
i liquid–mixture interface
L liquid
Nu value based on Nusselt's theory
o pure vapor ($W_\infty = 0$)
r reference
sat saturation
sep separation
v vapor
wall at the wall
∞ at the free stream.

1. Introduction

Condensation of vapors in the presence of noncondensable gases is an important topic due to its relevance to many industrial applications. Numerous investigations were carried out on this topic for the case of mixtures of a vapor and a heavier gas using different methods of solution and various simplifying assumptions. These investigations have demonstrated that the presence of a gas in the vapor stream can dramatically reduce the rate of heat transfer compared to the pure-vapor value.

By contrast, the case of mixtures of a vapor and a lighter gas received much less attention in the literature. The available results are limited [1–4]. Also, simplifying assumptions were used in these analyses that can limit their utility to certain flow conditions.

As a mixture of a vapor and a lighter gas flows downward along a vertical or inclined plate with condensation, a high gas concentration develops at the film–mixture interface causing the mixture density at the interface to be lower than the free-stream density. The difference between the buoyancy force and the gravity force at the interface gives rise to a net body force acting in the direction opposite to the flow direction. Since the interfacial gas concentration increases in the flow direction, this adverse net body force also increases in the flow direction, which may cause boundary-layer separation in the mixture. Solution of the boundary-layer equations in the liquid film and the mixture are valid only up to the separation point, and therefore it is important to be able to predict the separation location with good accuracy. The adverse net body force would also result in further reduction in heat transfer compared with the case of heavier gases where the net body force acts in the flow direction.

Denny and Jusionis [1] investigated the case of laminar film condensation from flowing vapor–gas mixtures along vertical isothermal plates. They solved the governing conservation equations in the mixture layer using a numerical technique. The model was simplified by neglecting the inertia forces and the convection terms in the momentum and energy equations of the liquid film, respectively. Further, they neglected conduction in the mixture layer, approximated the interfacial shear by $\tau_i = \dot{m}_i''(u_\infty - u_i)$, limited their analysis to cases of $Pr/Ja \gg 1$, i.e., small values of ΔT, and assumed uniform physical properties. All their results correspond to $W_\infty \leqslant 0.01$ and $\Delta T \leqslant 22^\circ$C. One of the mixtures considered in this analysis was Freon 12–air and these results will be compared later with the present model. Boundary-layer separation was not discussed in [1]. Later, Turner et al. [2] applied a similar model (e.g., no inertia or convection in the film, no sensible heat transfer in the mixture, no heat transfer due to diffusion in the mixture boundary layer) to the condensation of flowing liquid metals with noncondensable gases on a vertical isothermal plate. The boundary-layer equations were solved numerically using a coarse mesh with an estimated numerical uncertainty of 5–10%. For one of the mixtures (mercury–air), the results included the heat transfer rate and the separation length. These results will be referred to in a later section. A similarity solution was developed by Rutunaprakarn and Chen [3] for laminar film condensation of a quiescent vapor and a lighter gas with very small concentrations ($W_\infty \leqslant 5 \times 10^{-4}$) and uniform physical properties. This similarity solution is possible only for very small W_∞ and thus, may not be valid for most practical applications. Siddique et al. [4] reported a theoretical analysis for laminar film condensation of steam–hydrogen mixtures flowing over an isothermal horizontal plate. They extended a similarity solution developed earlier by Sparrow et al. [5] to include the sensible heat in the mixture using approximate closed-form correlations developed by Rose [6]. Among the other simplifying assumptions adopted by Siddique et al. are the elimination of inertia and convection in the liquid film, heat transfer due to mass diffusion in the mixture boundary layer and the interfacial thermal resistance. Uniform properties were assumed in order to facilitate the similarity solution,

The object of the present analysis is to apply the complete boundary-layer equations for the solution of steady, laminar film condensation (with a smooth interface) from flowing mixtures of a vapor and a lighter noncondensable gas on inclined isothermal plates. The emphasis would be placed on generating results for the separation length and the rate of heat transfer at high values W_∞ and ΔT, where previous analyses may not be applicable. Variation of properties in the streamwise and spanwise directions will be taken into consideration.

2. Governing equations and numerical method

The physical model is shown schematically in Fig. 1. A mixture of a vapor and a non-condensable lighter gas (velocity $= u_\infty$, temperature $= T_\infty$, and gas concen-

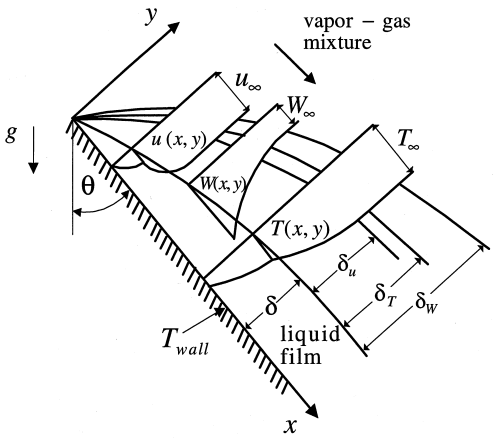

Fig. 1. Geometry and flow parameters.

tration = W_∞) flows parallel to an inclined isothermal plate of temperature T_{wall}. A layer of condensate liquid film forms with a variable thickness δ along the plate. As well, three boundary layers (hydrodynamic δ_u, thermal δ_T, and a concentration δ_W) form in the mixture with relative thicknesses dependent on Prandtl and Schmidt numbers. The flow is assumed to be laminar and steady in both the liquid and the vapor–gas mixture.

The isothermal plate is assumed to be very wide in the direction normal to the page and thus, the flow can be treated as two-dimensional. The total pressure, consisting of the partial pressures of the vapor and the gas, is assumed to be uniform throughout the flow domain. Ideal gas behavior was assumed for both the vapor and the gas. The x–y Cartesian coordinate system is shown in Fig. 1.

2.1. Governing equations

Conservation of mass, momentum, and energy within the liquid film results in the following equations, respectively,

$$\frac{\partial}{\partial x}(\rho_{\text{L}}u_{\text{L}})+\frac{\partial}{\partial y}(\rho_{\text{L}}v_L)=0 \tag{1}$$

$$\frac{\partial}{\partial x}(\rho_{\text{L}}u_{\text{L}}u_{\text{L}})+\frac{\partial}{\partial y}(\rho_{\text{L}}u_{\text{L}}v_{\text{L}})=\frac{\partial}{\partial y}\left(\mu_{\text{L}}\frac{\partial u_{\text{L}}}{\partial y}\right)+g(\rho_{\text{L}}-\rho_\infty)\cos\theta, \tag{2}$$

and

$$\frac{\partial}{\partial x}(\rho_{\text{L}}u_{\text{L}}C_{\text{P}_{\text{L}}}T_{\text{L}})+\frac{\partial}{\partial y}(\rho_{\text{L}}v_{\text{L}}C_{\text{P}_{\text{L}}}T_{\text{L}})=\frac{\partial}{\partial y}\left(k_{\text{L}}\frac{\partial T_{\text{L}}}{\partial y}\right) \tag{3}$$

Assuming that the vapor and the noncondensable gas are in thermal (same temperatures) and mechanical (same velocities) equilibrium, the governing equations of continuity, momentum, energy, and gas conservation for the vapor–gas mixture are:

$$\frac{\partial}{\partial x}(\rho u)+\frac{\partial}{\partial y}(\rho v)=0, \tag{4}$$

$$\frac{\partial}{\partial x}(\rho uu)+\frac{\partial}{\partial y}(\rho uv)=\frac{\partial}{\partial y}\left(\mu\frac{\partial u}{\partial y}\right)+g(\rho-\rho_\infty)\cos\theta, \tag{5}$$

$$\frac{\partial}{\partial x}(\rho uC_{\text{P}}T)+\frac{\partial}{\partial y}(\rho vC_{\text{P}}T)=\frac{\partial}{\partial y}\left(k\frac{\partial T}{\partial y}\right)+\frac{\partial}{\partial y}\left(\rho D(C_{\text{P}_{\text{g}}}-C_{\text{P}_{\text{v}}})\frac{\partial W}{\partial y}T\right), \tag{6}$$

and

$$\frac{\partial}{\partial x}(\rho uW)+\frac{\partial}{\partial y}(\rho vW)=\frac{\partial}{\partial y}\left(\rho D\frac{\partial W}{\partial y}\right). \tag{7}$$

In solving equations (1)–(7), the thermophysical property variation was taken into consideration by evaluating the properties at the local conditions. The properties varied as functions of temperature and mixture composition, as described in Section 2.3. The boundary conditions for equations (1)–(7) are as follows:

- At the plate surface ($y=0$)

$$u_{\text{L}}=v_{\text{L}}=0 \quad \text{and} \quad T_{\text{L}}=T_{\text{wall}} \tag{8}$$

- At the free stream ($y\to\infty$)

$$u=u_\infty, \quad T=T_\infty, \quad \text{and} \quad \text{W}=\text{W}_\infty \tag{9}$$

- At the liquid–mixture interface ($y=\delta$)

$$u_{\text{L}}=u, \tag{10}$$

$$\mu_{\text{L}}\frac{\partial u_{\text{L}}}{\partial y}=\mu\frac{\partial u}{\partial y}, \tag{11}$$

$$\dot{m}_i''=\rho_{\text{L}}u_{\text{L}}\frac{d\delta}{dx}-\rho_{\text{L}}v_{\text{L}}=\rho u\frac{d\delta}{dx}-\rho v, \tag{12}$$

$$k_{\text{L}}\frac{\partial T_{\text{L}}}{\partial y}=k\frac{\partial T}{\partial y}+\dot{m}_{\text{i}}''h_{\text{fg}}, \tag{13}$$

$$\dot{m}_{\text{i}}''W+\rho D\frac{\partial W}{\partial y}=0, \tag{14}$$

and

$$\dot{m}_{\text{i}}''=\frac{\sigma}{1-0.5\sigma}\frac{1}{\sqrt{2\pi RT_{\text{i}}}}[P_{\text{v}}-P_{\text{sat}}(T_{\text{i}})], \tag{15}$$

where the mass flux at the liquid–mixture interface is given by

$$\dot{m}_{\text{i}}''=\frac{\text{d}}{\text{d}x}\left(\int_0^\delta\rho_{\text{L}}u_{\text{L}}\,\text{d}y\right). \tag{16}$$

Equations (10)–(13) impose continuity of velocity, shear stress, mass flux, and heat flux at the liquid–mixture interface, respectively. Equation (14) insures that the liquid film is impermeable to the gas. A temperature jump may exist due to the interfacial resistance and equation (15) determines the magnitude of this jump (Mills [7]),

which was found to be significant only at low pressures. Equation (15) is based on the idea that the interfacial mass flux $\dot{m}_i''$ is proportional to the difference between the partial pressure of the mixture at the interface and the saturation pressure corresponding to the liquid-surface temperature. The condensation coefficient σ was taken to be unity, following the work of Turner et al. [2].

Governing equations (1)–(7) together with boundary conditions (8)–(15) provide a sufficient system for the calculation of the velocity, temperature, and gas concentration fields, as well as other important parameters such as the liquid film thickness, interfacial mass flux, and wall heat flux. The necessary input parameters are u_∞, T_∞, W_∞, T_{wall}, and the thermodynamic and transport properties of the vapor–gas mixture and the liquid film. Solutions were progressed along the plate up to the location where boundary-layer separation occurred, beyond which equations (1)–(7) are not valid. Boundary-layer separation in the mixture was assumed to occur at the location where the following conditions are satisfied:

$$\left.\frac{\partial u}{\partial y}\right|_{y=\delta} = 0 \quad \text{and} \quad u_{\text{i}} < u_\infty. \tag{17}$$

Progressing the solution beyond condition (17) will produce a negative mixture velocity relative to the interface in the region close to the interface while the mixture velocity relative to the interface is positive in the rest of the region.

The condition of laminar flow in the liquid film was also imposed by requiring the film Reynolds number Re_δ to remain below 30 up to the separation location. Film Reynolds number was calculated from the standard definition

$$Re_\delta = \frac{4\Gamma}{\mu_{\text{L}}}, \tag{18}$$

where Γ is the film flow rate per unit width, given by

$$\Gamma = \int_0^\delta \rho_{\text{L}} u_{\text{L}}\, \mathrm{d}y. \tag{19}$$

Values of μ_{L} and ρ_{L} in equations (18) and (19), respectively, were calculated at a reference temperature T_r, given by

$$T_r = T_{\text{wall}} + 0.31(T_\infty - T_{\text{wall}}). \tag{20}$$

The constant 0.31 in equation (20) was considered to be the value from the literature [8] that is most consistent with the present analysis.

2.2. Solution procedure

The numerical finite-control-volume approach of Patankar [9] was used in generating the solution. A mixture boundary-layer thickness δ_{mixture} was selected larger than that of any of the other boundary layers δ_u, δ_T, or δ_W. Selection of δ_{mixture} required a trial and error procedure since δ_u, δ_T, and δ_W were not known a priori. Care was exercised by selecting δ_{mixture} not much larger than the thickest of the other three layers in order to avoid unnecessary computations.

Since δ and δ_{mixture} vary along x, it was not possible to fit an orthogonal mesh over the flow domain in the x–y coordinate system. Therefore, the coordinate transformation

$$x = \chi \quad \text{and} \quad y = \delta\eta \tag{21}$$

was introduced and equations (1)–(7) were re-written in the χ–η coordinate system. An orthogonal mesh was fitted over the flow domain in the χ–η coordinate system and the transformed governing equations were discretized using the finite-control-volume method [9]. Because the equation set is parabolic, a marching technique was employed in the χ-direction, thus generating results at successive axial stations until boundary-layer separation was encountered.

At the leading edge of the plate the film thickness was set to zero and the free-stream conditions were imposed for the mixture. At the first axial station following the leading edge, the initial guesses used in the film were based on the classical Nusselt solution and the initial field values in the mixture were set equal to the free-stream values. Iterations based on the discretized equations were performed at the first axial station until convergence was achieved. The same iterative solution procedure was used at all subsequent axial stations except that the initial guess for the fields was taken as the converged solution from the previous station. Because of the coordinate transformation, it was more convenient to work with mass flow rates crossing the control-volume faces in the η-direction, $\dot{m}_{\text{L}}$ and $\dot{m}$, rather than the velocity components v_{L} and v. The solution procedure was to first calculate the liquid film thickness δ by solving the discretized form of equations (13), (15), and (16) simultaneously. Next, $\dot{m}_{\text{L}}$ and $\dot{m}$ were calculated from the discretized form of continuity equations (1) and (4) and then u_{L} and u were calculated from the discretized form of momentum equations (2) and (5). Values of $\dot{m}_{\text{L}}$ and $\dot{m}$ were then updated using the new values of u_{L} and u. Next, energy equations (3) and (6), and the gas conservation equation (7) were solved for the T_{L}, T, and W fields, respectively. Zero-thickness control volumes were placed at the wall, the interface, and the outer edge of the mixture layer in order to apply the boundary conditions in discretized form. At the end of each iteration, all field values were compared against their respective value from the previous iteration and two relative errors were calculated;

$$e_1 = \left|\frac{\phi_{\text{new}} - \phi_{\text{old}}}{\phi_{\text{new}}}\right|, \tag{22a}$$

and

$$e_2 = \left|\frac{\phi_{\text{new}} - \phi_{\text{old}}}{\phi_{\max} - \phi_{\min}}\right|. \tag{22b}$$

The value of e_1 was calculated for δ and values of e_1 and

e_2 were calculated for u_L, u, T_L, T, and W at all mesh points in the η-direction. Convergence was declared when either the maximum value of e_1 or the maximum value of e_2 was lower than 1×10^{-7} for all field variables.

Considerable numerical experimentation was conducted in order to insure that the results are mesh independent [10]. The typical mesh used in this study contains 300–400 equally-spaced subdivisions in the χ-direction, 40 equally-spaced subdivisions in the liquid film and 40–80 expanding subdivisions in the mixture layer. The sources of error in the numerical method have been minimized through the tests to obtain grid-independent results and through the use of tight convergence criteria and double precision variables in the computer code. The numerical diffusion introduced by upwind approximations is expected to have a negligible effect on the fine-grid results. Based on the numerical results obtained with different mesh configurations, it can be stated that the numerical uncertainty in the present results is within $\pm 0.1\%$.

2.3. Fluid properties

Computations were performed for three vapor–gas mixtures (steam–hydrogen, Freon 12–air, and mercury–air). In all the calculations described in this section, the liquid, vapor, and gas properties were functions only of temperature. Values of μ_L, C_{P_L}, k_L, C_{P_v}, and k_v for steam were found using linear interpolations from the tabulated data in Incropera and DeWitt [11]. The values of μ_v, C_{P_V}, and k_v for Freon 12 were calculated from least squares fits of the data in [12], while μ_L, C_{P_L}, and k_L were calculated from expressions given in [13]. The values of T_{sat}, P_{sat}, ρ_L, and h_{fg} for Freon 12 were correlated by the least squares method using tabulated values found in Avallone and Baumeister [14]. Functions provided by Irvine and Liley [15] were used to calculate T_{sat}, P_{sat}, ρ_L, and h_{fg} for steam as well as μ_g, C_{p_g}, and k_g for air. Air properties for temperatures below 250 K were obtained from Kays and Crawford [16] using linear interpolation. All properties for mercury were correlated by the least squares method using tabulated data found in Kakac et al. [17]. The densities of gas and vapor were obtained using the ideal gas equation of state. The mixture transport properties μ, k, and D were evaluated as functions of temperature, total pressure, and mixture composition following the procedure suggested by Reid et al. [18]. Standard additive procedures were used to calculate ρ and C_p. Details of the methods used to obtain all the correlations mentioned in this section can be found in [10].

2.4. Comparisons with previous studies

Comparisons were made between the results obtained from the present model and those reported earlier by Siddique et al. [4] for steam–hydrogen mixtures, Denny and Jusionis [1] for Freon 12–air mixtures, and Turner et al. [2] for mercury–air mixtures. The comparison with Siddique et al. is shown in Fig. 2 in terms of q/q_0 for forced-convection condensation on a horizontal flat plate at $T_\infty = 125\,^\circ$C, $3 \leqslant \Delta T \leqslant 70$ K, and $0.005 \leqslant W_\infty \leqslant 0.1$, where q_0 is the wall heat flux at $W_\infty = 0$. It is important to note that for the case of forced-convection condensation, the value of q/q_0 becomes independent of x. Figure 2 shows that the results from the present model agree very well with those of Siddique et al. at low values of ΔT (up to about 20 K). The deviation between the two models increases as W_∞ and/or ΔT increase. One possible reason for this trend is the assumption of constant properties and a constant value of Schmidt number in the analysis of Siddique et al. This assumption may be valid at low values of ΔT and W_∞, e.g., Schmidt number changes from 0.174 at the interface to 0.168 at the free stream for the data point corresponding to $\Delta T = 10$ K and $W_\infty = 0.005$ in Fig. 2. On the other hand, at $\Delta T = 70$ K and $W_\infty = 0.1$, Schmidt number changes from 0.778 at the interface to 0.298 at the free stream.

The comparison between the present analysis and that of Denny and Jusionis [1] for laminar film condensation of Freon 12–air on a vertical plate produced very good agreement with a maximum deviation of about 3% in the value of q/q_{Nu} along the plate [10]. However, the results reported by Denny and Jusionis and used in this comparison correspond to small liquid subcooling ($\Delta T < 20$ K) and small gas concentration ($W_\infty < 0.01$).

The third comparison is shown in Fig. 3 involving results from Turner et al. [2] and the present analysis for mercury-air mixtures condensing on a vertical isothermal plate at $T_\infty = 666.7$ K, $u_\infty = 0.305$ m s^{-1}, $\Delta T = 5.6$ and 16.7 K, and $W_\infty = 0.01$ and 0.03. Both sets of results are presented in terms of q/q_{Nu} along x up to the separation location. Figure 3 shows that the deviation between the two analyses can be significant in terms of the values of q/q_{Nu} and x_{sep}. The present results exhibit the expected behavior of small ΔT-effect on q/q_{Nu}. While this trend is not followed by the results of Turner et al. in Fig. 3, most

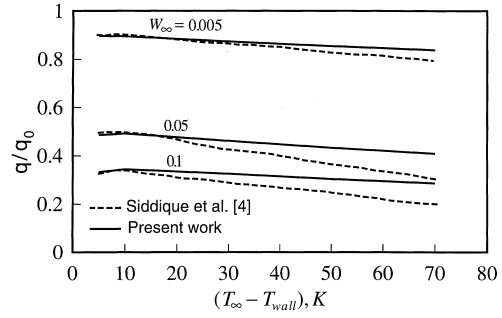

Fig. 2. Comparison with Siddique et al. [4] for steam–hydrogen at $T_\infty = 125^\circ$C.

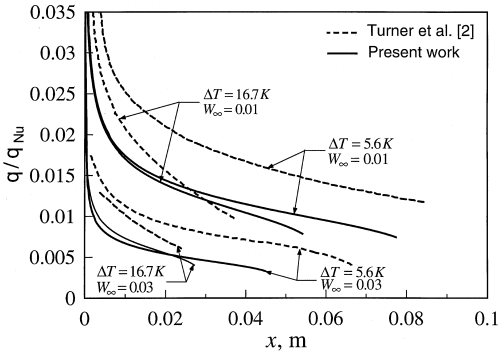

Fig. 3. Comparison with Turner et al. [2] for mercury–air at $T_\infty = 666.7$ K and $u_\infty = 0.305$ m s^{-1}.

of their other results (for other vapor–gas mixtures) were consistent with this trend. The deviation seen in Fig. 3 may be attributed to the combined effects of the simplifying assumptions adopted by Turner et al. in formulating their mathematical model and the coarse mesh (with high numerical uncertainty) used in their numerical solution, as discussed earlier in the Introduction.

3. Results and discussion

The three vapor–gas combinations considered in this study (steam–hydrogen, Freon 12–air, and mercury–air) correspond to vapor–gas molecular weight ratios of 9, 4.17, and 6.94, respectively. These three fluids were selected because they encompass a wide range of Prandtl numbers ($0.008 < Pr_L < 3.5$). For each vapor–gas combination, three values of T_∞ were used in order to cover a range of system pressure and for each T_∞, four values of ΔT were used in the calculations. A wide range of W_∞ (0–0.6 for steam–hydrogen and Freon 12–air, and 0–0.4 for mercury–air) was used for each combination of T_∞ and ΔT. The comparisons shown in Section 2.4 suggest that the present approach is particularly valuable for cases of high ΔT and W_∞ and therefore, the computation range was extended to these cases.

The results presented here include samples of velocity, temperature and concentration profiles, film thickness, separation distance, Nusselt number and film Reynolds number. A dimensionless approach was adopted in presenting these results. Following the transformations developed by Lucas [19], the nondimensional coordinate along the plate can be defined by,

$$x^* = \frac{xg\cos\theta}{u_\infty^2}. \tag{23}$$

A consequence of this transformation is that quantities such as δ^*, $Nu_x/Re_x^{1/2}$, and $Re_\delta/Re_x^{1/2}$ are dependent on x^* only for a given mixture. The validity of this transformation was confirmed numerically by generating results at the same x^* but different combinations of x, g, θ, and u_∞ and observing that the results would collapse [10]. Values of δ^*, Nu_x, and Re_x were calculated from the following definitions:

$$\delta^* = \delta\left[\frac{g\cos\theta}{u_\infty \nu_L}\right]^{1/2}, \tag{24a}$$

$$Nu_x = \frac{qx}{k_L(T_\infty - T_{wall})}, \tag{24b}$$

and

$$Re_x = \frac{u_\infty x}{\nu_L}, \tag{24c}$$

where

$$q = -\left(k_L\frac{\partial T_L}{\partial y}\right)\bigg|_{y=0}. \tag{24d}$$

The properties required in equations (24a–d) were evaluated at the reference temperature, T_r, given in equation (20), for the particular axial location of interest.

3.1. Detailed profiles

Figure 4 shows a representative sample of the velocity, concentration and temperature profiles for steam–hydrogen condensing on a vertical plate. These results correspond to $T_\infty = 100^\circ$C, $\Delta T = 15^\circ$C, $u_\infty = 0.05$ m s^{-1} and $W_\infty = 0.01$. It can be seen that the interfacial velocity and the thickness of the hydrodynamic boundary layer increase along x and that the interfacial slope of the velocity profile decreases down to zero at $x = x_{sep}$. The interfacial gas concentration increases in the flow direction and at each axial location, the concentration decreases nearly exponentially from the interfacial value to the free-stream value. As well, the thickness of the concentration boundary layer increases in the x direction. The sample temperature profiles demonstrate that the interfacial temperature decreases (consistent with the increasing W_i) while the thermal-boundary-layer thickness increases along x. All these trends were qualitatively the same for all mixtures and for all flow conditions.

3.2. Dimensionless film thickness

Results for the dimensionless film thickness of the three mixtures are shown in Fig. 5 for low values of ΔT and in Fig. 6 for high values of ΔT. In both figures, the results are given for wide ranges of W_∞, as indicated earlier. In examining these results, it is important to note that the solution approaches the forced-convection limit as x^* approaches zero and the free-convection limit is approached as x^* approaches infinity. In all results, the film thickness is seen to increase as we move from the forced-convection limit to the free-convection limit. The

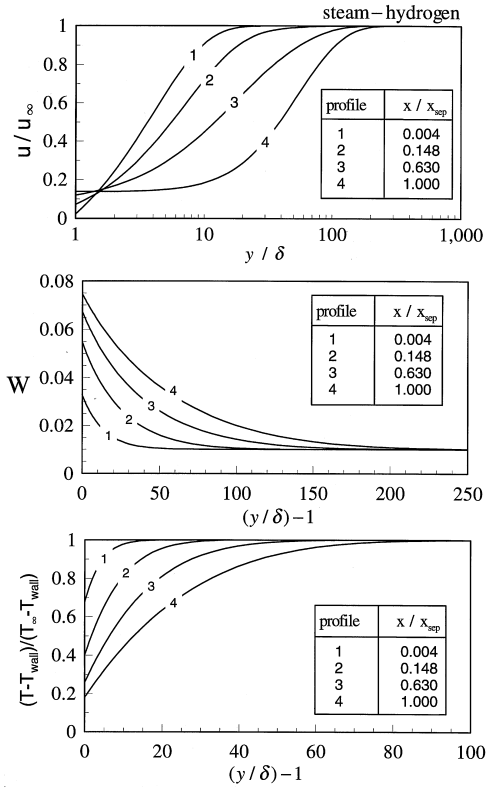

Fig. 4. Velocity, concentration and temperature profiles for steam–hydrogen condensing on a vertical plate at $T_\infty = 100°C$, $\Delta T = 15°C$, $u_\infty = 0.05$ m s^{-1} and $W_\infty = 0.01$.

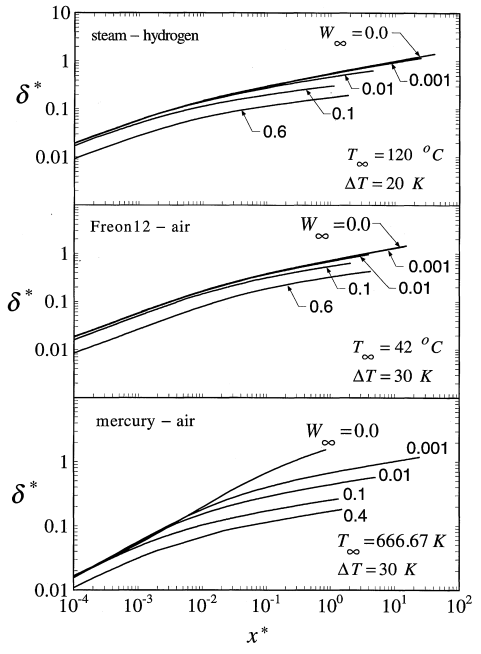

Fig. 5. Dimensionless film thickness for low values of ΔT.

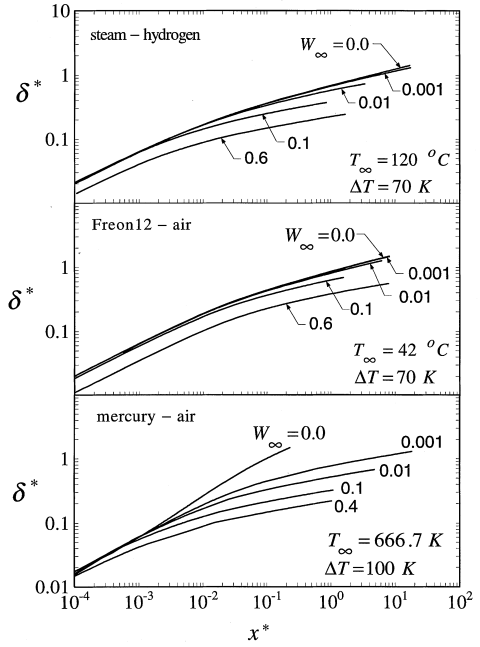

Fig. 6. Dimensionless film thickness for high values of ΔT.

influence of W_∞ is monotonic with δ^* decreasing with an increase in W_∞. The decrease in δ^* with W_∞ is more significant near the free-convective limit while at the forced-convective limit, this influence decreases to a negligible amount in some cases.

The effect of ΔT can be assessed by comparing the results in Figs 5 and 6. As expected, δ^* increases as ΔT increases while holding all other parameters unchanged. For all nonzero values of W_∞, the results are presented up to $x^* = x^*_{sep}$.

3.3. Separation distance

A major objective of this work is to investigate the separation phenomenon and its dependence on various parameters. Extensive results are presented in Figs 7–9 for the three mixtures under consideration with some interesting trends. For steam–hydrogen and Freon 12–air at any given combination of T_∞ and ΔT, the value of x^*_{sep} decreases with W_∞ up to a certain value (W_∞ between 0.2 and 0.3) beyond which x^*_{sep} increases with W_∞. Within the tested range, the value of T_∞ (which impacts on system pressure) appears to have a small effect on x^*_{sep}, while the effect of ΔT is much more significant. For mercury–air, the behavior of x^*_{sep} vs W_∞ is more intriguing than the other two mixtures with x^*_{sep} first increasing with W_∞, then decreasing and then increasing.

An attempt was made to explain the above trends in x^*_{sep}, at least in a qualitative manner. By combining equations (4) and (5), the conservation of momentum at the

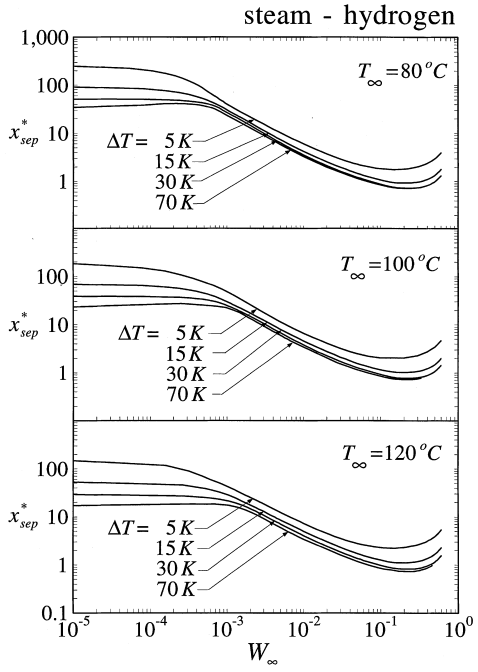

Fig. 7. Separation distance for steam–hydrogen.

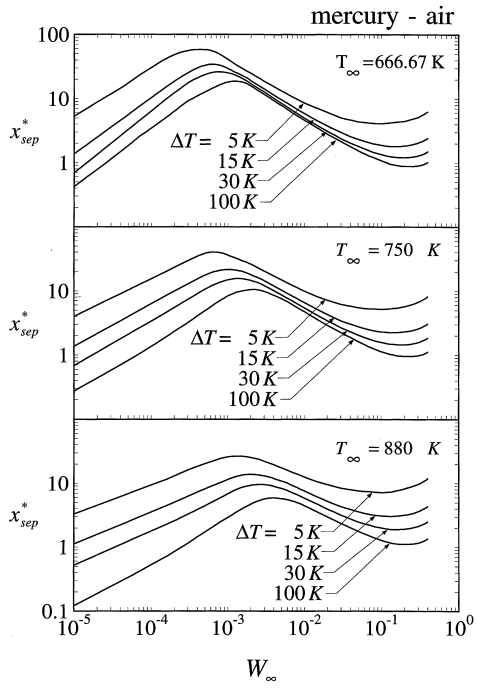

Fig. 9. Separation distance for mercury–air.

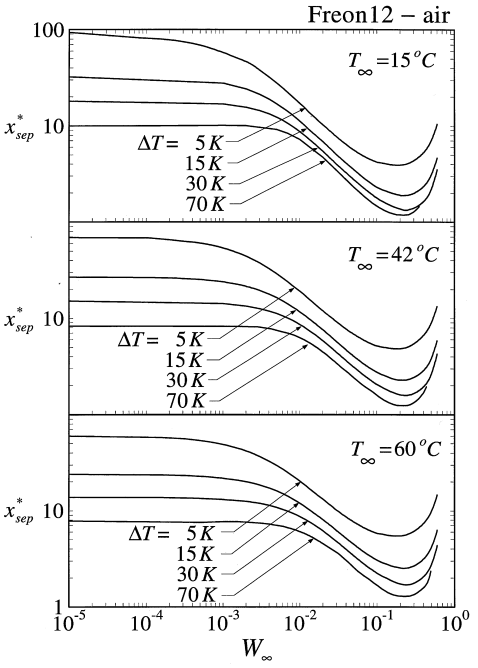

Fig. 8. Separation distance for Freon 12–air.

liquid–mixture interface can be written in the following form:

$$\mu_i\left(\frac{\partial^2 u}{\partial y^2}\right)_i = \rho_i u_i\left(\frac{\partial u}{\partial x}\right)_i + \rho_i v_i\left(\frac{\partial u}{\partial y}\right)_i + g(\rho_\infty - \rho_i)\cos\theta. \tag{25}$$

Three forces can be identified in the right-hand side of equation (25) corresponding to inertia of the interface, suction at the interface, and net body force, respectively. Each one of these forces varies in value along the plate and it is the combined effect of these three forces that determines the separation location. The net body force and the force due to inertia of the interface are adverse forces that promote separation, while the force due to interfacial suction acts to retard separation. The fact that the separation location is determined by the combined effect of these three axially varying forces makes this problem obviously much more complex than a simple boundary-layer problem for a fluid flowing over a stationary solid plate where the inertia and suction forces would not exist.

The terms in equation (25) were evaluated at the separation location (where $(\partial u/\partial y)_i = 0$) for some arbitrarily selected flow conditions and the results are shown in Fig. 10. These results demonstrate the variation of x^*_{sep}, $g(\rho_\infty - \rho_i)$ and $\mu_i(\partial^2 u/\partial y^2)_i$ with W_∞ for condensation on a vertical plate. The value of $\rho_i u_i(\partial u/\partial x)_i$ can be inferred from these results as the difference between $\mu_i(\partial^2 u/\partial y^2)_i$

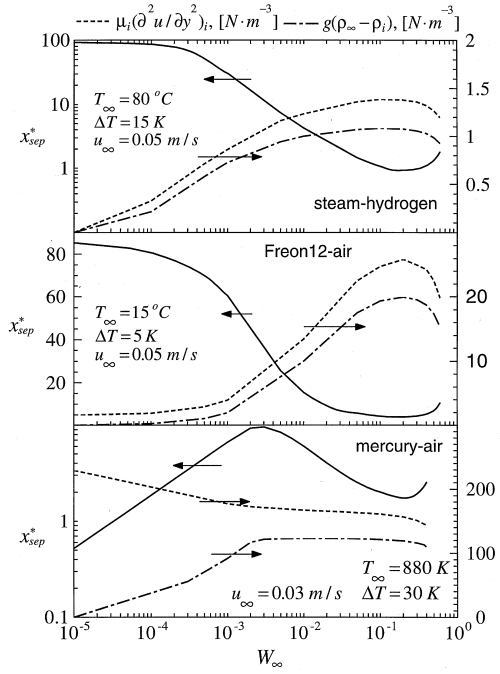

Fig. 10. Variation of the forces in equation (25) with W_∞ at the separation location for a vertical plate.

and $g(\rho_\infty - \rho_i)$. The behavior of the term $\rho_i v_i (\partial u/\partial y)_i$ upstream of the separation point and its variation with x and W_∞ were also investigated [10].

Figure 10 shows that, for steam–hydrogen and Freon 12–air, the net body force is dominant at the separation location and therefore, the behavior of x^*_{sep} vs W_∞ is determined mainly by the trend in the net body force. For both mixtures, an increase in the net body force results in a decrease in x^*_{sep} and vice versa. The magnitude of the force due to interfacial suction was found to decrease rapidly along the plate and also to decrease monotonically with W_∞. This force does not appear to have a strong role in shaping the trend of x^*_{sep} against W_∞.

For mercury–air, the situation is different. At low W_∞, the force due to inertia of the interface is dominant and since this adverse force starts out decreasing with W_∞, the value of x^*_{sep} starts out increasing with W_∞ up to a certain value of W_∞ (about 3×10^{-3} in Fig. 10). Over the region $3 \times 10^{-3} < W_\infty < 0.2$, the net body force and the interfacial inertia force remain nearly constant with W_∞. The reason for the net body force to remain constant over this region is that W_i is at or near its maximum value throughout this region and therefore $(\rho_\infty - \rho_i)$ does not change much until W_∞ increases beyond 0.2. In order to explore the reason for the decrease in x^*_{sep} over this region, the history of the term $\rho_i v_i (\partial u/\partial y)_i$ upstream of the separation point was examined and it was found that its absolute value at any x decreases significantly with W_∞, which explains the decrease in x^*_{sep}. Beyond $W_\infty = 0.2$, both the net body and interfacial inertia forces begin decreasing and consequently x^*_{sep} begins increasing with W_∞.

3.4. Heat transfer

Results of $Nu_x/Re_x^{1/2}$ for the three mixtures are presented in Fig. 11 for low values of ΔT and in Fig. 12 for high values of ΔT, covering a wide range of W_∞ in both figures. The devastating effect of W_∞ on Nu_x is clearly evident in these figures, particularly at high values such as $W_\infty = 0.4$–0.6, where the reduction in Nu_x can be orders of magnitude.

At any value of W_∞, the ratio $Nu_x/Re_x^{1/2}$ is seen in Figs 11 and 12 to approach a limiting value corresponding to forced-convection condensation at low values of x^*. Starting from this limiting value, $Nu_x/Re_x^{1/2}$ typically increases with x^* (particularly at low W_∞) due to the effect of gravity on the liquid film, which makes it thinner and faster. With further increase in x^*, the adverse effect of the net body force in the mixture layer starts to slow down the rate of increase of Nu_x with an actual reduction in the value of $Nu_x/Re_x^{1/2}$ typically occurring near the separation point. Considering the results in Figs 11 and 12 comparatively, the effect of ΔT on $Nu_x/Re_x^{1/2}$ appears to be small within the tested ranges, particularly when compared with the strong effect of W_∞.

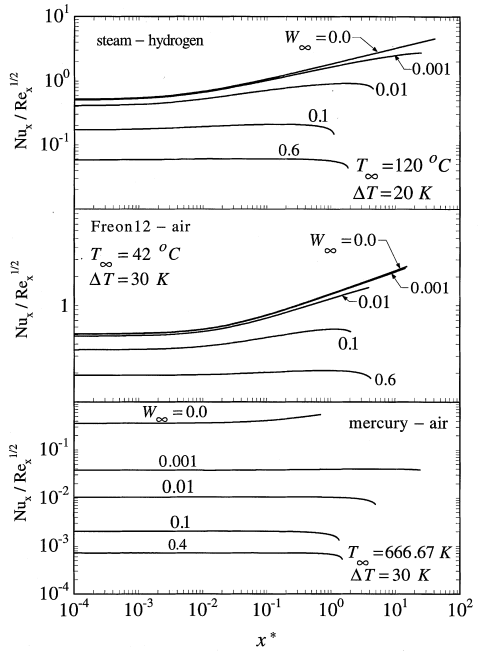

Fig. 11. Heat-transfer results for low values of ΔT.

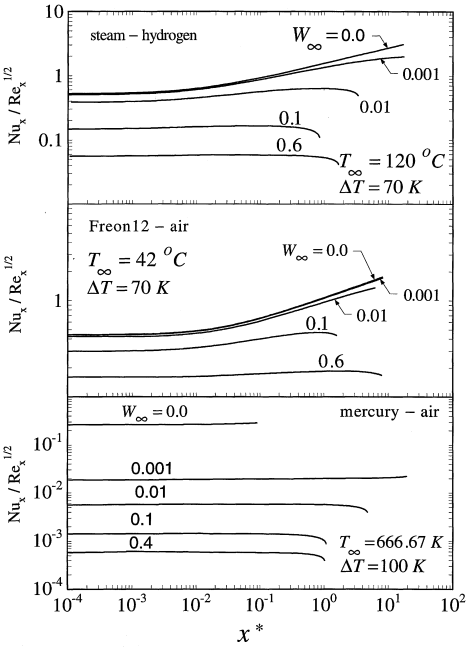

Fig. 12. Heat-transfer results for high values of ΔT.

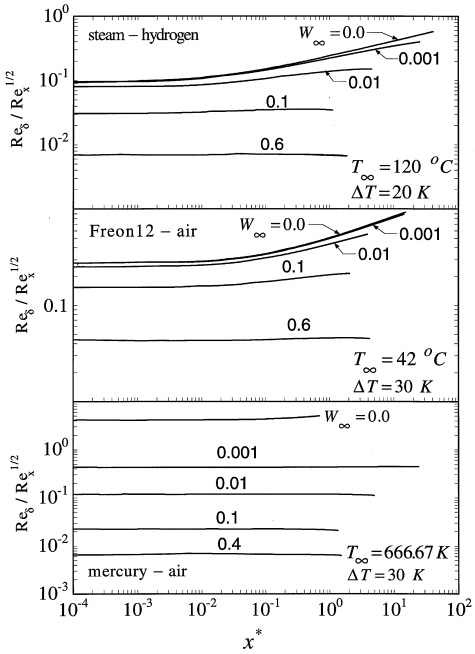

Fig. 14. Film Reynolds number for low values of ΔT.

A comparison between the heat transfer rate for steam–hydrogen and steam–air mixtures is shown in Fig. 13 at the same T_∞ (120°C), the same ΔT (20 K) and the same W_∞ (0.1 and 0.6). From these results, it is clear that lighter gases inhibit heat transfer even more than heavier gases. Also, $Nu_x/Re_x^{1/2}$ appears to increase continuously with x^* for steam–air due to the aiding effect of the net body force in the liquid film and mixture. On the other hand, for steam–hydrogen, the adverse effect of the net body force in the mixture is evident with increasing x^* and it ends up decreasing Nu_x near the separation point.

3.5. Film Reynolds number

All present results apply only to laminar film condensation. A well-accepted condition for the existence of laminar film flow with a smooth interface is $Re_\delta < 30$ [7].

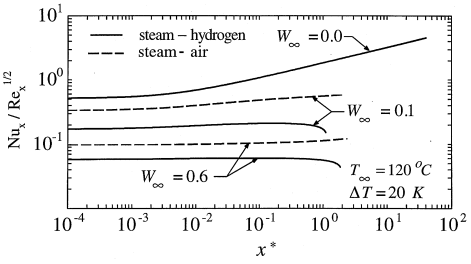

Fig. 13. A comparison between steam–hydrogen and steam–air.

Results are presented in Figs 14 and 15 in terms of $Re_\delta/Re_x^{1/2}$ vs x^*, from which the location x at which transformation from smooth laminar flow occurs can be determined for given values of u_∞, W_∞, T_∞, ΔT, and θ.

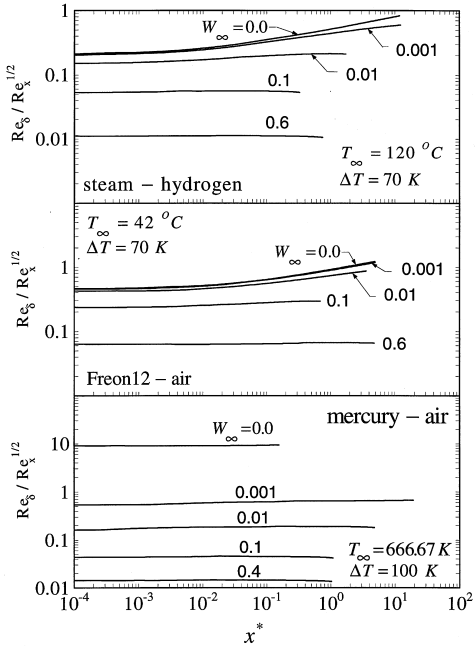

Fig. 15. Film Reynolds number for high values of ΔT.

These results illustrate that, for any vapor–gas mixture, the laminar region expands significantly as W_∞ increases due to the associated reduction in heat transfer. As well, comparing the results in Figs 14 and 15, it is clear that Re_δ increases with ΔT and consequently the length of the laminar region decreases with ΔT as expected.

4. Concluding remarks

A numerical, finite-control-volume approach has been utilized for solving the full set of two-phase boundary-layer equations for mixed-convection laminar film condensation on isothermal inclined plates in the presence of a lighter noncondensable gas. The model accounts for inertia and convection in the liquid film and mixture layer, as well as interfacial shear and thermal resistance. Therefore, there is no restriction on the applicability of the model in terms of fluid properties (high or low liquid Prandtl numbers) or the type of noncondensable gas. Also, the solution technique is extendible to different free-stream conditions (constant or varying u_∞ and W_∞) and different wall conditions (constant or varying wall temperature).

Solutions were obtained for three vapor–gas mixtures encompassing the range $0.008 < Pr_L < 3.5$ and vapor–gas molecular weight ratios of 4.17–9. Comparison with previously published results based on simplified models showed that good agreement is possible only for low values of ΔT and W_∞. Results from the present model are presented in dimensionless form (up to the point of separation) for different values of T_∞ (system pressure) and wide ranges of W_∞ and ΔT. Extensive results are presented for the separation distance x^*_{sep} at various conditions. Interesting trends were noted in the variation of x^*_{sep} with W_∞; these trends were discussed and explained. The heat-transfer values experience significant reduction due to the presence of the gas. It is shown that the reduction in heat transfer is more pronounced for lighter gases than for heavier gases.

Acknowledgement

The financial assistance provided by the Natural Sciences and Engineering Research Council of Canada is gratefully acknowledged.

References

[1] V.E. Denny, V.J. Jusionis, Effects of noncondensable gas and forced flow on laminar film condensation, International Journal of Heat and Mass Transfer 15 (1972) 315–326.
[2] R.H. Turner, A.F. Mills, V.E. Denny, The effect of non-condensable gas on laminar film condensation of liquid metals, Journal of Heat Transfer 95 (1973) 6–11.
[3] O. Rutunaprakarn, C.J. Chen, Effect of lighter non-condensable gas on laminar film condensation over a vertical plate, International Journal of Heat and Mass Transfer 18 (1975) 993–996.
[4] M. Siddique, M.W. Golay, M.S. Kazimi, The effect of hydrogen on forced convection steam condensation, AIChE Symposium Series No. 269 85 (1989) 211–216.
[5] E.M. Sparrow, W.J. Minkowycz, M. Saddy, Forced convection condensation in the presence of noncondensables and interfacial resistance, International Journal of Heat and Mass Transfer 10 (1967) 1829–1845.
[6] J.W. Rose, Approximate equations for forced convection condensation in the presence of a noncondensing gas on a flat plate and a horizontal tube, International Journal of Heat and Mass Transfer 23 (1980) 539–546.
[7] A.F. Mills, Heat Transfer. Irwin, Homewood, IL, 1992.
[8] W.J. Minkowycz, E.M. Sparrow, Condensation heat transfer in the presence of noncondensables, interfacial resistance, superheating, variable properties, and diffusion, International Journal of Heat and Mass Transfer 9 (1966) 1125–1144.
[9] S.V. Patankar, Numerical Heat Transfer and Fluid Flow. Hemisphere, New York, NY, 1980.
[10] V. Srzic, Modeling of mixed-convection laminar film condensation from mixtures of a vapor and a lighter non-condensable gas. M.Sc. thesis, University of Manitoba, 1997.
[11] F.P. Incropera, D.P. DeWitt, Fundamentals of Heat and Mass Transfer, 4th ed., John Wiley, New York, NY, 1996.
[12] ASHRAE, Handbook of Fundamentals. SI ed., 1997, p. 19.5.
[13] ASHRAE, Thermophysical Properties of Refrigerants, 1976, p. 11.
[14] A.E. Avallone, T. Baumeister, Mark's Standard Handbook for Mechanical Engineers, McGraw-Hill, 9th ed., New York, 1987, pp. 4–45.
[15] T.F. Irvine, Jr. P.E. Liley, Steam and Gas Tables with Computer Equations. Academic Press, London, U.K., 1984.
[16] W.M. Kays, M.E. Crawford, Convective Heat and Mass Transfer. McGraw-Hill, New York, NY, 1993.
[17] S. Kakac, R.K. Shah, W. Aung, Handbook of Single-Phase Convective Heat Transfer. John Wiley, New York, NY, 1987.
[18] R.C. Reid, J.M. Prausnitz, T.K. Sherwood, The Properties of Gases and Liquids. McGraw-Hill, New York, NY, 1977.
[19] K. Lucas, Combined body force and forced convection in laminar film condensation of mixed vapours—integral and finite difference treatment, International Journal of Heat and Mass Transfer 19 (1976) 1273–1280.